Available online at www.sciencedirect.com

ScienceDirect

Procedia Engineering 102 (2015) 1531 – 1538

Procedia Engineering

www.elsevier.com/locate/procedia

The 7th World Congress on Particle Technology (WCPT7)

Towards hydrodynamic simulations of wet particle systems

Sudeshna Roy[a*], Stefan Luding[a], Thomas Weinhart[a]

[a]*Faculty of Engineering Technology, MESA+, University of Twente, P. O. Box 217, 7500 AE Enschede, The Netherlands*

Abstract

This paper presents the rheology of weakly wetted granular materials in the slow frictional regime, using Discrete Element Method (DEM) simulations. In a split-bottom ring shear cell geometry a slow, quasi-static deformation leads to wide shear bands away from the walls. Dry non-cohesive and cohesive materials are compared in order to understand the effect of liquid bridge capillary forces on the macroscopic flow properties. Different liquid contents lead to different flow curves when measuring the shear stress-strain relations, helping to understand the effect of wetness on the flow of granular materials.

Selection and peer-review under responsibility of Chinese Society of Particuology, Institute of Process Engineering, Chinese Academy of Sciences (CAS)

Keywords: DEM; Shear band; Liquid bridge; Slow flow rheology

1. Introduction

When granular materials are subjected to slow shear, the relative motion is confined to a narrow region called shear band, a zone of large strain rates between non-sheared regions. Shear bands are observed in many complex materials like foams, emulsions, colloids and granular materials, which often experience inter-particle attractive forces of different physical origins. These forces may be in the form of *Van der Waals* forces for small dry grains, capillary forces due to presence of moisture, coagulation or sintering of particles and many more. Extensive studies have been done to understand the effect of dry cohesive contact forces on the steady-state shear band formation [1]. Such studies also focus on adhesive and non-adhesive emulsions [2, 3]. Most recently, attempts have been made to better understand the behavior of wet granular media involving migration of liquid away from the shear band [4, 5].

* Sudeshna Roy. Tel.: +31-(53)-489-3301
E-mail address: s.roy@utwente.nl

Selection and peer-review under responsibility of Chinese Society of Particuology, Institute of Process Engineering, Chinese Academy of Sciences (CAS)
doi:10.1016/j.proeng.2015.01.288

Nomenclature

R_i, R_s, R_o	inner/ split/ outer radius of shear cell [m]
H	filling height [m]
(r, Ψ, z)	cylindrical coordinates [m, degree, m]
$\langle r \rangle$	mean radius of particles [m]
δ	overlap [m]
V_b	volume of liquid bridge [m^3]
θ	contact angle [degree]
γ	surface tension [kgs^{-2}]
τ	shear stress [Pa]
p	hydrostatic pressure [Pa]
$\dot{\gamma}$	strain rate [s^{-1}]

It has been observed that the homogeneous presence of liquid bridges, when prohibiting migration across the contacts, affects the shear band structure [6] and different liquid bridge models were compared [7]. In this paper, we aim to draw a comparison between dry and weakly wetted granular materials and thereby better understand the effects of capillary forces on the macroscopic properties.

2. Model System Geometry

Split- Bottom Ring Shear Cell: The geometry of the system consists of an outer cylinder (radius R_o = 110 mm) rotating around a fixed inner cylinder (radius R_i = 14.7 mm) with a rotation frequency of f_{rot} = 0.01 s^{-1}. The granular materials are confined by gravity between the two concentric cylinders, a bottom plate, and a free top surface. The bottom plate is split at radius R_s = 85 mm into a moving outer part and a static inner part. Fig. 1 shows a sketch of the set-up [8]. Due to the split at the bottom, a stable shear band is formed at the bottom and it widens as it goes up. Due to the geometry chosen, the shear band formed is wide and curves inwards [9]. An intermediate filling height (H = 40 mm) is chosen so that the shear band reaches the free surface and does not reach the inner wall. In order to save computation time, only a quarter of the system ($0° \leq \Psi \leq 90°$) with periodic boundary conditions in the angular coordinate is simulated [10].

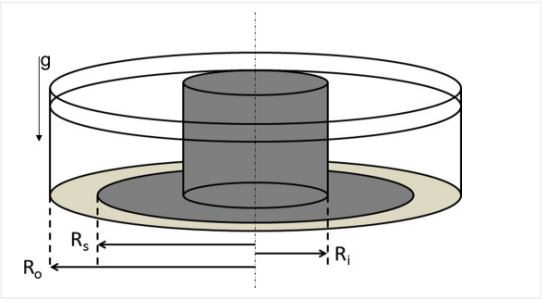

Fig. 1: Split-Bottom Ring Shear Cell set-up.

Model parameters: The system is filled with $N \approx 3.7 \times 10^4$ spherical particles of density ρ = 2,000 kg/m^3. The average radius of the particles is $\langle r \rangle$ = 1.1 mm with a homogeneous size distribution (with r_{min}/r_{max} = 1/2) of width $1 - (\langle r \rangle^2 / \langle r^2 \rangle) = 0.18922$. A linear contact model is used to describe the interaction of particles with contact stiffness k = 100 Nm^{-1} when they are in contact. The short range non-contact linear and non-linear interactive forces are described in sec. 4. In order to study the influence of liquid bridge contact forces in the pendular regime (the

change to the funicular regime occurs at 10 % < saturation < 20 % of the pore volume [11]), we analyze the system for liquid bridge volumes $V_b \in$ [0, 4.2, 20, 42, 130] nl. The maximum volume of liquid bridge of 130 nl corresponds to saturation of 4 % of the pore volume, which is still in the range of the pendular regime. The contact friction is set to $\mu = 0.01$, i.e. quite small, in order to be able to focus on the effect of contact liquid bridge adhesion only.

3. Micro-macro Transitions

The macroscopic properties such as angular velocity, strain rate, shear stress, hydrostatic pressure, apparent shear viscosity and the inertial number which fields in r and z directions can be calculated by micro-macro transition methods from the DEM results [6, 12]. The averaging time interval is 3 s, with a discrete averaging time step of 0.25 s. The results are obtained after running the simulation for 9 s. The averaging is performed with a spacing of $\Delta r \approx 0.0025$ and $\Delta z \approx 0.0025$ in the radial and vertical directions, respectively, and we fully average over the angular direction.

4. Interaction Models

The particle properties and the interaction force models are inserted in a DEM simulation. Many possible models exist in the literature [13 – 18]. However, only the linear normal and tangential contact model [13], linear irreversible adhesive force model [14] and one liquid capillary bridge model [15 – 18] are the focus of discussion here.

4.1. Linear Normal Contact Model

Two particles i and j, with radii r_i and r_j, respectively, interact mechanically only when they are in contact so that their overlap [14, 18]

$$\delta = (r_i + r_j) - \left|\hat{a}_i - \hat{a}_j\right| \tag{1}$$

is positive, $\delta > 0$, with $\hat{a}_i$ and $\hat{a}_j$ the positions of the centre of the particles. The simplest normal contact model takes into account linear repulsive and dissipative forces

$$f_n = k\delta + \gamma_n v_n \tag{2}$$

with a spring stiffness k, a viscous damping coefficient γ_n and the relative velocity in normal direction v_n.

4.2. Tangential Force Model

The model implemented for tangential contact forces and torques includes friction, rolling resistance and torsion as described in ref. [13, 19]. The simplest tangential friction force model can be described as

$$f_t = k_t \delta_t + \gamma_t v_t \tag{3}$$

where k_t is the tangential spring stiffness, γ_t the tangential viscous damping and v_t the relative velocity in tangential direction. The tangential force is limited by the Coulomb sliding coefficient of friction as

$$f_t \leq \mu f_n \tag{4}$$

4.3. Linear Irreversible Contact Model

A linear irreversible force contact model is used for dry adhesive materials [14, 19]. Long-range interaction forces are present when dry adhesive particles collide, i.e. forces are present for negative overlap δ also. Such interaction forces may be reversible or irreversible depending on the type of adhesive force acting during approach. In the irreversible adhesive contact model, the adhesive force is established when the particles come into contact, so short-range non-contact ($\delta \leq 0$) adhesive forces are only active during unloading and separation of particles [14]. So the overall force law during approach can be written as

$$f = \begin{cases} 0, & \delta \leq 0 \\ -f_0 + f_n, & \delta > 0 \end{cases} \tag{5}$$

During unloading and separation the force can be written as

$$f = \begin{cases} 0, & \delta \leq -f_o/k_c \\ -f_0 - k_c\delta, & -f_0/k_c < \delta \leq 0 \\ -f_0 + f_n, & \delta > 0 \end{cases} \tag{6}$$

where f_o is the maximum adhesive force and k_c is the "stiffness" of adhesion force.

4.4. Liquid Bridge Capillary Force Model

A liquid capillary bridge force contact model is a combination of the same contact model as for linear irreversible contact model and a liquid bridge with the approximation of Willett et al. [15] to calculate the interacting forces. The liquid bridge capillary force acts between the particles once the contact is established and when they are separating. The magnitude of liquid bridge capillary force depends on the volume of the liquid bridge between the particles, the contact angle θ = 20º, surface tension γ = 0.020 Nm^{-1}, the effective radius of the particles r_{eff} and the inter-particle distance $s = -\delta$. With these parameters we approximate the inter-particle force f_c of the capillary bridge according to the proposal of Willett et al. [15], who computed the exact capillary force as a function of separation distance by numerically solving the Laplace - Young equation. The results are fitted by a polynomial to obtain the capillary forces as a function of the scaled separation distance

$$f_c = \begin{cases} 2\pi\gamma r_{eff}\cos\theta/(1 + 1.05\hat{s} + 2.5\hat{s}^2), & s \geq 0 \\ 2\pi\gamma r_{eff}\cos\theta, & s < 0 \end{cases} \tag{7}$$

where $\hat{s} = s\sqrt{r/V_b}$. The effective radius of two spherical particles of unequal size can be estimated as the harmonic mean of the two particle radii. Thus the effective radius is $r_{eff} = (2r_i r_j)/(r_i + r_j)$. Here V_b is the volume of the liquid bridge. The bridge ruptures and f_c becomes zero when the separation distance is more than a critical distance called the rupture distance. The rupture distance is defined as

$$s_{crit} = r_{eff}\left(1 + \frac{\theta}{2}\right)\left[\left(\frac{V_b}{r_{eff}^3}\right)^{\frac{1}{3}} + 0.1\left(\frac{V_b}{r_{eff}^3}\right)^{\frac{2}{3}}\right] \tag{8}$$

So the overall force law during approach can be written as

$$f = \begin{cases} 0, & \delta \leq 0 \\ -f_c + f_n, & \delta > 0 \end{cases} \tag{9}$$

During unloading and separation the force can be written as

$$f = \begin{cases} 0, & \delta \leq -s_{crit} \\ -f_c, & -s_{crit} < \delta \leq 0 \\ -f_c + f_n, & \delta > 0 \end{cases} \quad (10)$$

5. Results

In this section, we present our results of DEM simulations. We analyze the rheology and shear banding in our system for different operating conditions and then interpret the observed effects.

5.1. Linear irreversible adhesive forces

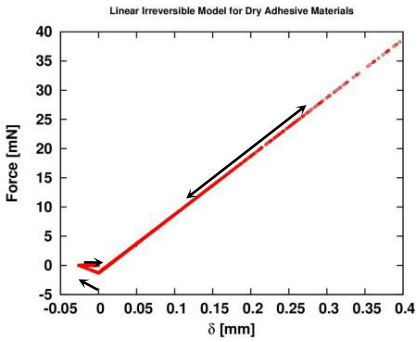

Fig. 2: Scatter plots of overlaps and forces between all contacts. The arrows indicate the direction of loading and unloading.

Fig. 2 displays scatter plots of the inter-particle forces as a function of overlaps between the interacting particles for dry adhesive materials following the linear irreversible contact model as described in sec. 4.3. The maximum adhesive force f_o at $\delta = 0$ is 0.0013 N and k_c is 50 N/m, which amounts to the same adhesive energy for one unloading as corresponding to a 42 nl liquid bridge volume.

5.2. Structure and distribution of liquid bridge capillary forces

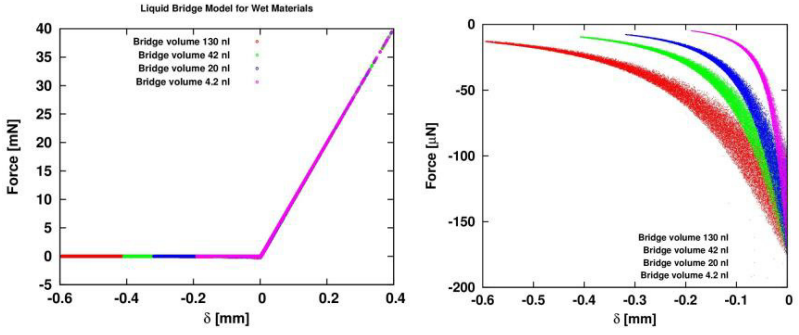

Fig. 3: (a) Scatter plots of overlaps and forces between all contacts and (b) scatter plots of overlaps and forces for $\delta \leq 0$ when the liquid bridge capillary force is active.

Fig. 3 displays scatter plots of the inter-particle forces as a function of overlaps between the interacting particles for wet materials with different capillary bridge volumes. Each point here corresponds to a contact and the color represents the different volumes of liquid bridges. This represents the capillary force effects for 4.2 nl, 20 nl, 42 nl and 130 nl volume of liquid bridges. Fig. 3 (a) corresponds to the plot for the interacting forces during approach, loading, unloading and separation. Fig. 3 (b) corresponds only to the active liquid bridge capillary force region when $\delta \leq 0$. When the particles are in contact, the force magnitude is independent of the liquid bridge volume. As the separation distance increases, the liquid bridge capillary force magnitude decreases. The energy loss to overcome the cohesive forces is proportional to the volume of the liquid bridge. The scatterings are due to the polydispersity of the particles.

5.3. Shear Band

The slit in the bottom wall at $R = R_s$ triggers a relative motion of particles in the form of shear band. In order to study the dynamic steady flow behavior of the material, the shear band structure is analyzed. The angular velocity profile at a given height can be well approximated by an error function [20]

$$\frac{\omega(r)}{2\pi f_{rot}} = \frac{1}{2}\left(1 + \operatorname{erf}\left(\frac{r - R_c}{W}\right)\right) \tag{11}$$

where R_c and W are the position and the width of the shear band at height z, respectively. The shear band structure for dry and wet materials is shown in Fig. 4.

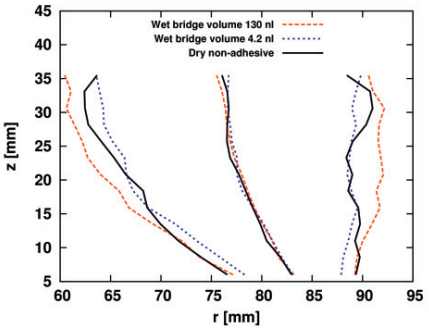

Fig. 4: Shear band structure for dry non-adhesive and wet materials. R_c and $R_c \mp W$ are plotted for different heights. The different colors correspond to dry (black solid), 4.2 nl (blue dotted) and 130 nl (red dashed) liquid bridge volumes respectively.

Variations in volume of the liquid bridge introduce noticeable changes in the shear band structure. The shear band gets wider for higher volume of liquid but the position remains relatively unchanged.

5.4. Effect on macroscopic properties

The shear resistance of granular materials is a result of friction and interlocking of particles. So the shear resistance may even increase if the inter-particle cohesive forces exist between the particles since they enhance the resistance to tension [20]. In Fig. 5 (a), the yield shear stress as a function of normal stress is shown for dry non-adhesive material using linear normal contact model and for different volumes of the liquid bridges. For dry material, the slope is fitted to obtain the macroscopic friction coefficient μ_m. The addition of liquid bridge force results in higher yield shear stress magnitudes and as a result an offset c is observed in the plot. This offset is referred to as the macroscopic cohesive strength c. While dry data are fitted well with $c = 0$, the fitted cohesive strength increases with increasing liquid bridge volume, as shown in Fig. 5 (b). The addition of liquid bridge forces leads to larger shear stress magnitudes and as a result the macroscopic yield stress at critical state is shifted upwards at given high

pressure. At lower pressure, however, the differences in shear stress between dry and wet media are not so prominent. From the plot, the local shear stress $|\tau|$ at higher pressures can be considered as a linear function of hydrostatic pressure p. So it can be written as

$$|\tau| = \mu_m p + c \tag{12}$$

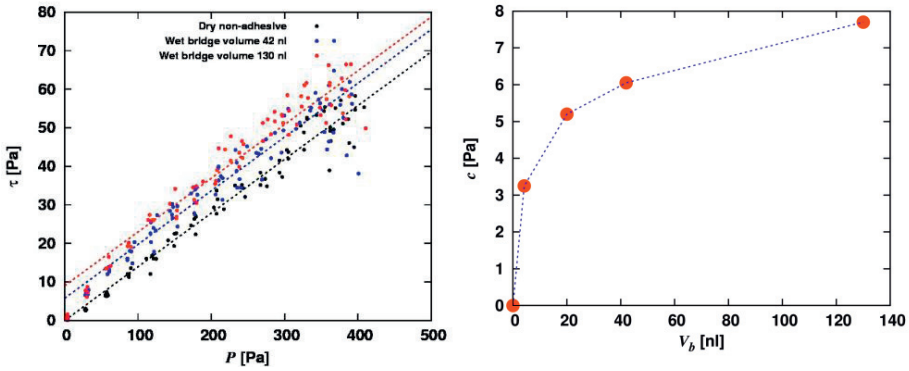

Fig. 5: (a) Local Shear Stress $|\tau|$ plotted against local pressure p. The data corresponds to strain rate $\dot{\gamma} > 0.08$ s^{-1}. The different color corresponds to dry non-adhesive (black), 42 nl (blue) and 130 nl (red) liquid bridge volume respectively. The solid lines represent the function $|\tau| = \mu_m p + c$, with the macroscopic friction coefficient $\mu_m = 0.14$ (b) shows the macroscopic cohesive strength c as a function of the liquid bridge volume.

Fig. 6 shows a comparison of macroscopic cohesive strength for the dry non-adhesive material, the dry adhesive material with irreversible non-contact force and the wet material for 42 nl bridge volume.

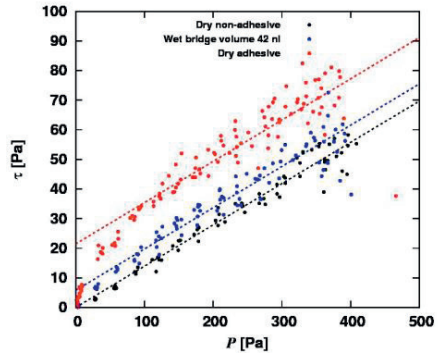

Fig. 6: Local Shear Stress $|\tau|$ plotted against local pressure p. The data corresponds to strain rate $\dot{\gamma} > 0.08$ s^{-1}. The different color corresponds to dry non-adhesive (black), 42 nl (blue) and dry adhesive (red) models. The solid lines represent the function $|\tau| = \mu_m p + c$, with the macroscopic friction coefficient $\mu_m = 0.14$.

The macroscopic cohesive strengths for different contact models are different even when the magnitudes of adhesive energy are equal as discussed in sub secs. 5.1 and 5.2. Thus it is concluded that the total adhesive energy is not the controlling parameter for the macroscopic adhesive strength. It remains to find out the parameters at the microscopic level for both the dry adhesive and the wet systems that give the same macroscopic cohesive strength.

6. Conclusion

The simulations in this paper compare the flow behavior of dry non-cohesive and cohesive model granular materials with weakly wetted granular materials. It is concluded that a small volume liquid bridge can significantly affect the flow behavior of the materials by increasing the width of the shear band. The addition of a small volume of liquid to the materials increases the critical shear stress of the materials at high pressure. A simpler model system with shorter range but same energy dissipation during unloading astonishingly leads to much larger yield stress. In future, we would also like to study the effect of higher liquid volumes on the shear stress at low pressure and understand the correlations between the dry and wet adhesive forces for different force models.

Acknowledgements

Helpful discussions with A. Singh, A. Gladkyy and R. Schwarze are gratefully acknowledged. The authors also acknowledge the financial support of STW through the STW (DFG joint) project # 12272.

References

[1] S. Luding, F. Alonso-Marroquin, The critical-state yield stress (termination locus) of adhesive powders from a single numerical experiment, Granular Matter 32 (2) (2011), 109 – 119.
[2] S. R. Hohler, S. Cohen-Addad, A multiscale model for the slow viscoelastic response of liquid foams, Journal of Physics: Condensed Matter 17 (2005), R1041 – R1069.
[3] G. Ovarlez, S. Rodts, X. Chateau, P. Coussot, Phenomenology and physical origin of shear-localization and shear-banding in complex fluids, Rheologica Acta 48 (2009), 831.
[4] R. Mani, D. Kadau, D. Or, H. J. Herrmann, Fluid depletion in shear bands, Phys. Rev. Lett. 109 (2012), 248001-1 – 5.
[5] R. Mani, D. Kadau, H. J. Herrmann, Liquid migration in sheared unsaturated granular media, Granular Matter 15 (2013), 447 – 454.
[6] R. Schwarze, A. Gladkky, F, Uhlig, S. Luding, Rheology of weakly wetted granular materials – a comparison of experimental and numerical data, Granular Matter 15 (6) (2013), 455 – 465.
[7] A. Gladkky, R. Schwarze, Comparison of different capillary bridge models for application in the discrete element method, (2014).
[8] D. Fenistein, M. V. Hecke, Kinematics - wide shear zones in granular bulk flow, Nature (2003), 425.
[9] T. Unger, J. Torok, J. Kertesz, D. E. Wolf, Shear band formation in granular media as a variational problem, Phys. Rev. Lett. 92 (2004), 214301-1 – 4.
[10] S. Luding, The effect of friction on wide shear bands, Particulate Science and Technology 26 (2008), 33 – 42.
[11] A. Denoth, The pendular-funicular liquid transition in snow, Journal of Glaciology 25 (1980), 93 – 97.
[12] S. Luding, From microscopic simulations to macroscopic material behaviour, Computer Physics Communications. 147 (2002), 134 – 140.
[13] S. Luding, Introduction to Discrete Element Methods: Basics of Contact Force Models, European Journal of Environmental and Civil Engineering- EJECE 12 (2008), 785 – 826.
[14] A. Singh, V. Magnanimo, S. Luding, Mesoscale contact models for sticky particles, submitted to Powder Technology (2013).
[15] C. D. Willett, M.J. Adams, S.A. Johnson, J. P. K. Seville, Capillary Bridges between Two Spherical Bodies, Langmuir. 16 (24) (2000), 9396 – 9405.
[16] Y. I. Rabinovich, M. S. Esayanur, B. M. Moudgil, Capillary Forces between Two Spheres with a Fixed Volume Liquid Bridge: Theory and experiment, Langmuir 21 (2005), 10992 – 10997.
[17] S. Herminghaus, Dynamics of wet granular matter, Advances in Physics 54 (2005), 221 – 261.
[18] T. Weigert, S. Ripperger, Calculation of the Liquid Bridge Volume and Bulk Saturation from the Half-filling Angle, Particle and Particle Systems Characterization 16 (1999), 238 – 242.
[19] S. Luding, Cohesive frictional powders: contact models for tension, Granular Matter 10 (2008), 235 – 246.
[20] A. Singh, V. Magnanimo, K. Saitoh, S. Luding, Effect of cohesion on shear banding in quasistatic granular material, Phys. Rev. E 90 (2014), 022202-1 – 14.